Hyperfine Interactions 113 (1998) 59–79

Nuclear inelastic scattering

Aleksandr Chumakov and Rudolf Rüffer

European Synchrotron Radiation Facility (ESRF), B.P. 220, F-38043 Grenoble Cedex, France

The development of the new field of nuclear inelastic scattering is reviewed. The experimental technique and the variety of applications are illustrated by recent results obtained at the Nuclear Resonance beamline of the European Synchrotron Radiation Facility.

1. Introduction

Nuclear inelastic scattering is a new domain in the field of nuclear resonant scattering of synchrotron radiation. Observed few years ago for the first time, nuclear inelastic scattering became the subject of intensive studies, because of its ability to provide information on the lattice dynamics, not available otherwise. In Mössbauer spectroscopy the rigidity of the atomic lattice is measured by the Lamb–Mössbauer factor (f_{LM}), i.e., the recoilless fraction of resonant absorption of γ-rays by nuclei. The lattice dynamics is studied by the supplemental factor of recoil fraction ($1 - f_{\mathrm{LM}}$). Nuclear inelastic scattering opened the way to go beyond this single parameter and provided access to the energy spectrum of the recoil, i.e., to the frequency distribution of lattice vibrations. For a long time this has been the domain of inelastic neutron and nowadays also inelastic X-ray scattering. Not competing with these techniques in the measurement of dispersion relations, nuclear inelastic scattering provides complementary information: direct measurement of the density of phonon states. Due to the large nuclear cross-section, the count rate in nuclear inelastic scattering experiments is quite high, up to $\sim 10^2$ counts per second. Therefore the measurements may be performed very fast, typically during several hours. This is a distinct advantage of the new technique compared to inelastic neutron and X-ray scattering.

In this paper we review the development of nuclear inelastic scattering and outline the main results, achieved at several synchrotron radiation facilities. A short survey of the theory of nuclear inelastic scattering is included. In addition, we illustrate the experimental technique and the variety of applications with the recent results, which were obtained at the Nuclear Resonance beamline [1] of the European Synchrotron Radiation Facility.

2. From an idea to the experiment

The specific features of nuclear inelastic scattering are well illustrated by the history of its development. Nuclear inelastic scattering is an edifying example of the technique, which was proposed long before it became possible, mostly forgotten, and independently found later.

After Mössbauer's discovery of recoilless nuclear resonant scattering and understanding that the recoil fraction of scattering is determined by lattice dynamics, it was immediately proposed to extend Mössbauer spectroscopy for measurements of the phonon spectra [2]. However, the significant experimental difficulties were outlined:

(i) In order to scan an energy range of about ± 50 meV with the technique of Doppler shift, one needs the velocity of ~ 1 km/s.

(ii) The energy range of the phonon spectrum is typically 10^6–10^7 times broader than the width of nuclear level. Due to the "spreading" of the probability of inelastic interaction over this energy range the cross section of inelastic scattering is weak. Thus a very intense radiation beam is required, typically 10^6–10^8 photons/s.

(iii) High background of transmitted or electronically scattered radiation should be overcome.

It was not possible to solve these problems in the frames of conventional Mössbauer spectroscopy, therefore the experiment was never performed.

In 1985 the first excitation of nuclear levels with synchrotron radiation was unambiguously demonstrated in [3]. The use of synchrotron radiation is extremely favorable for nuclear inelastic scattering. Firstly, the continuous spectrum of synchrotron radiation permits easy energy scans. Secondly, the spectral density of synchrotron radiation is sufficiently high. Finally, the pulsed structure of synchrotron radiation allows one to separate the delayed nuclear response from the prompt electronic scattering. Thus synchrotron radiation offers an impressive possibility to overcome all the difficulties mentioned above at once.

Since that time the required instrumentation was developed. The high-resolution monochromators [4–6], which were elaborated in order to decrease the intensity of the prompt flash in timing experiments, provided perfect spectrometers for the energy scans. The new avalanche photo diode detectors were found [7,8], which were capable to count the delayed nuclear photons despite of the extremely intensive flash of prompt electronic scattering.

The observation of nuclear inelastic scattering was for a large extent prepared by the experiments on time evolution of incoherent nuclear scattering. The progress in this field has been achieved in parallel efforts of several groups [9–12]. Already the first experiment [9] showed, that the time evolution of incoherent scattering contains, besides the replica of the time pattern of elastic forward scattering, an exponentially decaying component of inelastic scattering.

For the first time nuclear inelastic scattering was revealed during an energy scan as a broadening and a slight shift of the resonant peak in the energy dependence of

incoherent nuclear scattering of 23.9 keV radiation by a ^{119}Sn foil [13,14]. In spite of the small effect (the energy resolution was ∼35 meV), it was properly attributed to the inelastic interaction with the phonons. For the ^{57}Fe isotope monochromators with better energy resolution were already elaborated [6], therefore the experiment was repeated with the 14.4 keV radiation of ^{57}Fe, where completely convincing results were obtained [15]. The energy spectrum of nuclear recoil agreed with the calculations, based on the density of phonon states, available from neutron scattering.

The procedure to treat the experimental data has been elaborated [16]. It includes the normalization of the energy spectrum of nuclear recoil, the accurate determination of the Lamb–Mössbauer factor from the area of the inelastic part of the spectrum, and the direct determination of the normalized density of phonon states. The studies of the dynamics of Mössbauer isotopes in solids [1,15–17,23–25], fluids [18], proteins [19,20], and nano-particles [21,22] were performed. The temperature dependence of nuclear inelastic scattering was investigated [1,21,23,24]. Experiments with single crystals revealed a possibility to measure separately the lattice vibrations along different crystallographic directions [25]. The theory of inelastic nuclear scattering, previously available only for the cubic Bravais lattice [26], was extended to the general case of anisotropic crystals [27]. The further development of the method is performed at several sources of synchrotron radiation: European Synchrotron Radiation Facility (France), Advance Photon Source (USA) and National Laboratory for High Energy Physics (Japan). This year the SPring-8 source (Japan) comes to operation.

3. Instrumentation

Nuclear inelastic scattering exploits the special features of synchrotron radiation as high collimation of the X-ray beam and its pulsed time structure. We discuss the typical experimental set-up of this technique with an example of the Nuclear Resonance beamline [1], ID18, of the ESRF (figure 1). A monochromatic beam of X-rays with an ∼eV bandwidth is prepared by the standard beamline equipment, among them the undulator and the high-heat-load pre-monochromator being the most important items. Further monochromatization down to ∼meV bandwidth is achieved with the high-resolution monochromator.

The beam of X-rays, which energy is close to the resonance energy of the nuclear transition, irradiates a sample and excites the resonant nuclei. The radiation, which

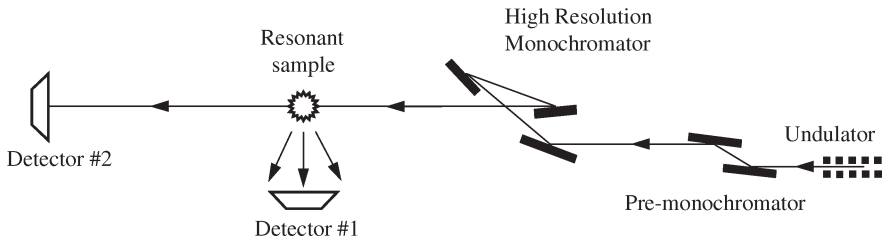

Figure 1. Experimental set-up for the measurements of nuclear inelastic absorption.

results from nuclear de-excitation, has to be distinguished from other photons, which pass through the sample without interaction or are scattered by the electrons. This is achieved utilizing the time distribution of the scattered radiation. The yield of nuclear scattering is delayed due to the finite lifetime of the nuclear excited state, whereas the electronic scattering is essentially prompt on that time scale. Fast electronics is synchronized with the revolutions of the electron beam in the storage ring and it counts only the events between the pulses of incident radiation. Thus only the delayed quanta, which result from nuclear scattering, are detected.

Nuclear scattering is counted by two avalanche photo diode (APD) detectors [28,29] (figure 1). The first detector is located close to the sample. It counts the quanta, scattered in a large solid angle. The second detector is located far away from the sample. It counts the quanta, scattered by the nuclei in forward direction. These two detectors follow two qualitatively different processes of nuclear scattering. Being scattered inelastically, the photon acquires a certain phase shift and, therefore, is no longer coherent with the incident radiation. If the phase shift is random for various nuclei, the scattering is spatially incoherent over the nuclear ensemble, and the scattered photon may be associated with some particular nucleus. The products of de-excitation of the single nucleus are emitted in a large solid angle as spherical waves (neglecting the polarization effects). Thus the first detector monitors the energy spectrum of inelastic excitation via counting the incoherent scattering of radiation by localized nuclei (figure 2a).

The second detector monitors nuclear forward scattering [31,32]. The paths of the waves, scattered by various nuclei in forward direction are indistinguishable, therefore the waves from all nuclei have the same phases, and the scattering is spatially coherent. The scattered photon cannot be associated with some particular nucleus, but is produced by collective scattering of radiation by large nuclear ensemble. This is an elastic process, because any energy transfer would destroy the coherence. Thus with the second detector one measures the energy profile of *elastic* scattering. An example is shown in figure 2b. It is essentially the instrumental function of the monochromator, because the width of the nuclear level in this scale is negligible. On-line monitoring of the instrumental function simplifies the processing of the experimental data and provides the precise reference for the energy position of the nuclear resonance.

Comparing the instrumentation of nuclear inelastic scattering to inelastic neutron [33] or X-ray scattering [34,35], one may note that the set-up for nuclear inelastic scattering benefits much from the narrow width of the nuclear resonance. Other inelastic techniques deal twice with the problem of monochromatization: a highly monochromatic beam has to be prepared to irradiate the sample, and the energy of the scattered radiation has to be analyzed. The energy transfer is determined as a shift of the energy of the scattered radiation *relative to the energy of the incident radiation*. The narrow width of nuclear levels ($\sim$neV) makes the nuclear resonance itself an ideal energy reference, therefore either the monochromator or the analyzer section of the conventional inelastic scattering set-up may be omitted. Usually it is preferable to omit the analyzer. In this scheme (figure 1) the energy of the incident radiation is varied in the vicinity of the nuclear transition by scanning the angle of the high-resolution

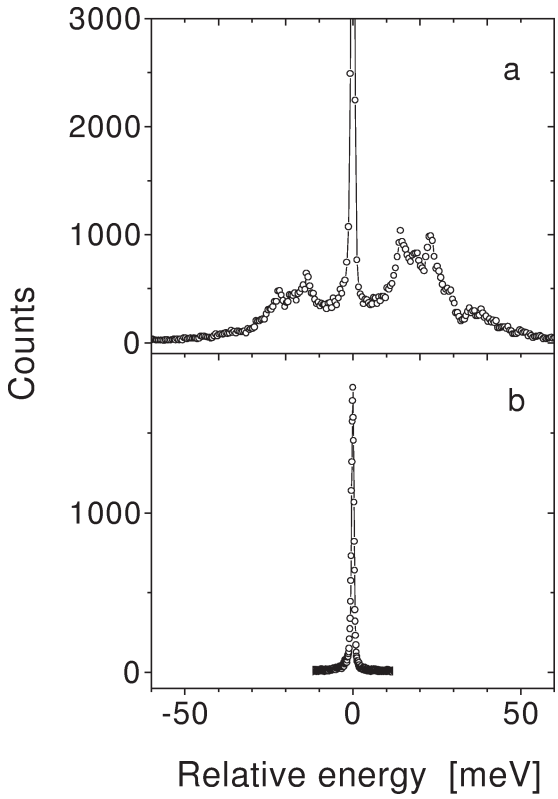

Figure 2. An example of the experimental data: (a) energy spectrum of nuclear inelastic absorption in the $^{57}Fe_3BO_6$ crystal, measured with the energy resolution of 0.82 meV. The data are obtained with an improved set-up of the three-crystal monochromator described in [30]; (b) the instrumental function of the monochromator. The solid lines are to guide the eye.

monochromator and the energy dependence of inelastic interaction is monitored via the intensity of incoherent nuclear scattering. The energy transfer is determined as a shift of the incident energy *relative to the energy of nuclear transition*, which is "marked" by the elastic channel of nuclear forward scattering (figure 2b). The energy resolution is determined only by the monochromator. Figure 1 schematically shows the high resolution monochromator for the particular case of the instrument, described in [30]. Several other schemes are available [6,36,37].

4. Nuclear inelastic scattering and nuclear inelastic absorption

Above we denoted the technique as "nuclear inelastic scattering". This is a convenient characteristic of the method relative to inelastic neutron or X-ray scattering. However, it is not completely precise and may be misleading if one would interpret it as a definition of the involved process.

An excited nucleus, which results from either elastic or inelastic excitation, may decay via two channels: radiative decay and internal conversion. Decaying via the radiative channel the nucleus emits γ-ray fluorescence radiation. The relative probability of this channel is $1/(1+\alpha)$, where α is the conversion coefficient of the nuclear transition. The energy of the emitted γ-radiation may be precisely equal the energy of the nuclear transition (elastic emission), or shifted by the energy of the accompanied phonon (inelastic emission). When the nucleus decays via the channel of internal conversion, the energy of nuclear excited state is transmitted to an electron of the atomic shell. This conversion electron leaves the atom, and the remaining hole results in the subsequent emission of atomic X-ray fluorescence radiation and/or Auger electrons. The relative probability of this channel is $\alpha/(1+\alpha)$. For most of the Mössbauer isotopes $\alpha \gg 1$, therefore internal conversion is the dominating channel.

In general, one can use the expression "scattering" for both channels of nuclear decay. However, the two channels are differently influenced by lattice dynamics, therefore it is worthwhile to distinguish them clearly. Below we reserve the expression "scattering" only for the radiative channel, where the absorbed photon results in the re-emitted γ-ray photon, whereas for the non-radiative channel we use the more conventional expression "absorption".

Specific experimental schemes may be chosen in order to measure either nuclear inelastic *absorption* or nuclear inelastic *scattering*. If the products of internal conversion are detected (X-ray fluorescence radiation, conversion or Auger electrons), one measures the cross-section of nuclear inelastic absorption. The location of the detector relative to the incident beam does not matter, since the angular distribution of the atomic emission is an entirely atomic property and does not depend on the "history" of nuclear excitation. Thus the allowed momentum transfer is not specified by the experimental set-up. The phonons with any momentum, which is allowed by the dispersion relations for a particular energy transfer, contribute equally to nuclear absorption. Therefore nuclear absorption provides an ideal "momentum-integrated" tool for the measurement of lattice dynamics.

If the γ-ray photons of the radiative channel are detected (i.e., if one studies specifically inelastic "scattering"), the analysis becomes more complicated. The momentum transfer, which is defined by the specific location of the detector, and the energy of the scattered radiation has to be considered.

Until now most of the reported works [15–25] were performed under the experimental conditions, where X-ray fluorescence radiation was the dominating contribution to the collected signal (one exception of electron emission [38] is worth mentioning). This means that the studied channel was *nuclear inelastic absorption*. The contribution of γ-ray fluorescence radiation is only about few percent for the typical experimental conditions [39]. This is caused by the dominating probability of the internal conversion channel, the higher efficiency of the detectors for the softer X-ray fluorescence radiation, and trapping of γ-ray fluorescence radiation in the sample [39].

Several attempts to investigate specifically nuclear inelastic *scattering* were performed, but no definite results were yet reported. Although it was the *scattering* process,

which has been utilized in the first observation of nuclear inelastic excitation [13,14], however, the energy resolution in that early work was not sufficient for the quantitative analysis of the data. An important question in these studies is the feasibility of *coherent nuclear inelastic scattering*. One may suppose that if the energy transfer is defined, the scattered γ-ray photons are emitted along the specific directions, which are determined by the momentum transfer via phonon dispersion relations. However, in contrast to neutron scattering, the characteristic time of nuclear scattering is much longer than the phonon lifetime. Therefore although a large number of nuclei can be involved into the particular mode of lattice vibration, the coherence of the waves, scattered by various nuclei is preserved only during very short time. Then in analogy to nuclear scattering under the diffusion conditions [11,40] one may expect an extremely fast ($\sim 10^{-12}$ s) decay of coherent nuclear inelastic scattering, which would make its observations difficult.

5. Theory

We discuss only the theory of nuclear inelastic *absorption*, and do not consider the case of inelastic *scattering*. The theory of nuclear inelastic absorption was elaborated in the 1960's [26] on the basis of the theory of incoherent inelastic neutron scattering [41].

The energy dependence of the probability of nuclear inelastic absorption $S(E)$ can be expressed in terms of a multi-phonon expansion [26]:

$$S(E) = \mathrm{e}^{-2W}\left[\delta(E) + \sum_{n=1}^{\infty} \frac{(2W)^n}{n!} A_n(E)\right]. \tag{1}$$

Here the Dirac δ-function $\delta(E)$ describes the elastic part of absorption, and the nth term of the expansion represents the inelastic absorption accompanied by creation (annihilation) of n phonons. The coefficient e^{-2W} is the Lamb–Mössbauer factor, where

$$2W = E_{\mathrm{R}} \int_0^{\infty} \frac{g(E)}{E} \frac{1 + \mathrm{e}^{-\beta E}}{1 - \mathrm{e}^{-\beta E}}\, \mathrm{d}E, \tag{2}$$

$g(E)$ is the density of phonon states; $\beta = (k_{\mathrm{B}}T)^{-1}$, k_{B} is the Boltzmann constant, T is the temperature; $E_{\mathrm{R}} = \hbar^2 k^2/2M$ is the recoil energy of a free nucleus; k is the wave vector of the X-ray photon; and M is the mass of the nucleus. The one-phonon term in eq. (1) is given by the expression

$$A_1(E) = \frac{E_{\mathrm{R}} g(|E|)}{2WE(1 - \mathrm{e}^{-\beta E})}, \tag{3}$$

and the subsequent terms under harmonic approximation may be found through the recursive relation

$$A_n(E) = \int_{-\infty}^{+\infty} A_1(E')A_{n-1}\big(E - E'\big)\,\mathrm{d}E'. \tag{4}$$

Comparing eqs. (2), (3) with the corresponding expressions in [26,41], one should be aware of the opposite definitions of the positive energy for inelastic nuclear and neutron scattering.

One can check that for all n the terms A_n are normalized according to

$$\int_{-\infty}^{+\infty} A_n(E)\,\mathrm{d}E = 1; \tag{5}$$

therefore the complete probability of nuclear absorption is also normalized:

$$\int_{-\infty}^{+\infty} S(E)\,\mathrm{d}E = \mathrm{e}^{-2W}\sum_{n=0}^{\infty}\frac{(2W)^n}{n!} \equiv 1. \tag{6}$$

The relative contribution of the n-phonon term is given by $(2W)^n/n! = (-\ln f_{\mathrm{LM}})^n/n!$. If the Lamb–Mössbauer factor is close to unity, the expansion in eq. (1) converges rapidly and only few terms of multi-phonon contribution are significant. These contributions can be revealed in the experimental data (figure 3). If the Lamb–Mössbauer factor is small, then a large number of terms has to be taken into account, and the interpretation of the expansion (1) as the sum of multi-phonon processes becomes meaningless.

Eqs. (1), (3), (4) have the advantage that they give directly the relative contributions of the various multi-phonon processes. For the purpose of the experimental data

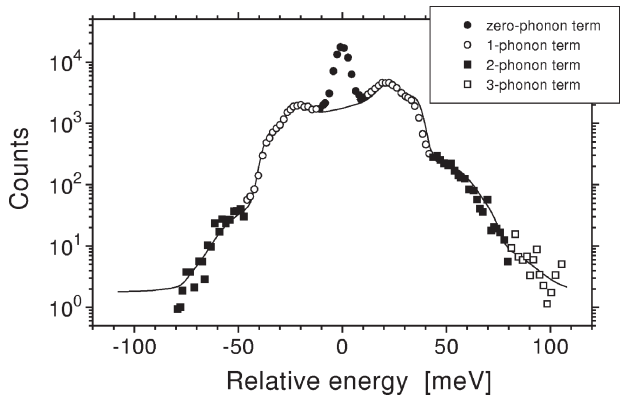

Figure 3. Multi-phonon contributions to nuclear inelastic absorption in α-iron. Different markers show the regions of the spectra, where the corresponding contributions are dominant. The solid line is the calculation according to eqs. (7)–(9) with the density of phonon states, obtained from neutron scattering [42].

analysis it is convenient to simplify them. The coefficient ($2W$) can be canceled, and eqs. (1), (3), (4) are rewritten as:

$$S(E) = f_{\mathrm{LM}} \left(\delta(E) + \sum_{n=1}^{\infty} S_n(E) \right), \tag{7}$$

$$S_1(E) = \frac{E_{\mathrm{R}} g(|E|)}{E(1 - \mathrm{e}^{-\beta E})}, \tag{8}$$

$$S_n(E) = \frac{1}{n} \int_{-\infty}^{+\infty} S_1\big(E'\big) S_{n-1}\big(E - E'\big)\, \mathrm{d}E'. \tag{9}$$

Note that here the n-phonon contributions $S_n(E)$ are no longer normalized.

The coefficient $1/(1-\mathrm{e}^{-\beta E})$ in the one-phonon term is a single expression, which describes the occupation of phonon states in the case of both phonon annihilation ($E < 0$) and phonon creation ($E > 0$). One can check that for the phonon annihilation part of the spectrum this coefficient is equivalent to n_{B}, whereas for phonon creation part it equals ($n_{\mathrm{B}} + 1$), where $n_{\mathrm{B}} = 1/(\mathrm{e}^{\beta|E|} - 1)$ is the Bose occupation factor. For any particular energy the ratio of phonon creation and phonon annihilation probability is given by $(n_{\mathrm{B}} + 1)/n_{\mathrm{B}} = \mathrm{e}^{\beta|E|}$.

The experimental energy spectra of nuclear inelastic absorption would be directly proportional to the probability $S(E)$, which is given by the expression (1), if the yield of atomic fluorescence is a linear function of the absorption cross-section. This is not valid for the central elastic peak, because of large saturation due to the high cross-section of elastic absorption [16] and the influence of the forward scattering on the yield of atomic fluorescence [9–12]. However, the linear approximation does hold for the inelastic part of the energy spectrum, because the cross-section of inelastic scattering is small (e.g., $\sim 10^{-25}$ cm^2 for ^{57}Fe). Then one may use the obvious normalization

$$\int_{-\infty}^{-0} S(E)\, \mathrm{d}E + \int_{+0}^{+\infty} S(E)\, \mathrm{d}E = (1 - f_{\mathrm{LM}}) \tag{10}$$

and find both the density of phonon states and the Lamb–Mössbauer factor from the experimental data in iterative calculations using eqs. (1), (2) and (10). This, for instance, is the conventional method of processing the data in incoherent inelastic neutron scattering [43].

However, one can benefit from the precise "momentum-integrated" feature of nuclear inelastic absorption and use the sum rules in order to obtain the direct normalization of the experimental spectrum [16]. According to Lipkin's sum rule [44] the first momentum of the energy spectrum of inelastic absorption equals the mean recoil energy E_{R} of a free nucleus. One may use this rule in order to normalize the experimental data, because the central peak is essentially symmetric and does not contribute to the first momentum. The corrections on the possible asymmetry of the instrumental

function may also be taken into account [16]. From the normalized spectrum one can calculate the Lamb–Mössbauer factor according to eq. (10), subtract the multi-phonon contributions either by iterative procedure or via Fourier transformation [27,45] and derive the density of phonon states from the one-phonon term according to eq. (8). The reliability of the results may be checked by the alternative calculation of the Lamb-Mössbauer factor using eq. (2) and the obtained density of phonon states [23,25,27]. Application of sum rules for the higher momenta of the experimental energy spectrum provides further information on the kinetic and potential energy of lattice vibrations [44,46].

The theory above is valid for polycrystalline samples and for single crystals with a mono-atomic cubic unit cell [26]. In the case of an anisotropic single crystal the mathematical apparatus is similar, but the derived density of phonon states becomes "projected" on the wave vector of the incident photon [27].

6. Temperature dependence

Temperature dependence of nuclear inelastic absorption is largely determined by the temperature dependence of the occupation of phonon states. As discussed in the previous section, the probability of inelastic absorption with energy gain (left-hand side of the spectrum) is proportional to the Bose occupation factor $n_{\mathrm{B}} = 1/(\mathrm{e}^{\beta|E|} - 1)$, whereas the probability of inelastic absorption with energy loss (right-hand side of the spectrum) is proportional to $(n_{\mathrm{B}} + 1)$. An obvious meaning of these coefficients is that the X-ray quantum may gain energy only from an existing phonon, whereas it may lose energy to an existent phonon or for the creation of a new phonon. At high temperature $n_{\mathrm{B}} \approx (n_{\mathrm{B}} + 1)$, so the spectra of inelastic absorption are approximately symmetric. At low temperature n_{B} approaches zero, whereas $n_{\mathrm{B}} + 1$ approaches unity, therefore the spectra become very asymmetric. The temperature dependence of the asymmetry of the spectra was studied in several experiments [1,21,23,24].

Figure 4 shows the temperature dependence of nuclear inelastic absorption in α-iron [23]. At $T = 400$ K the thermal energy k_{B}T is $\sim$34 meV, therefore the occupation is relatively high for all phonon states, and the energy spectrum of inelastic absorption has only a small asymmetry (figure 4). At $T = 24$ K the thermal energy is only $\sim$2 meV, so the phonon states with the energy above, e.g., $\sim$10 meV are not occupied. Thus no inelastic absorption can be traced in the energy-gain part of the spectrum (figure 4). However, inelastic absorption with energy loss still remains possible, because the recoil may excite the phonons even in the frozen lattice.

Besides the temperature-dependent probability of the occupation of states, the temperature dependence of inelastic nuclear absorption may arise from the temperature dependence of the density of states. Most pronounced variation occurs in the vicinity of phase transitions. Figure 5 shows the temperature dependence of inelastic nuclear absorption in the $[^{57}\mathrm{Fe(bpp)_2}][\mathrm{BF_4}]_2$ sample, where the ligand bpp is 2,6-bis (pyrazol-

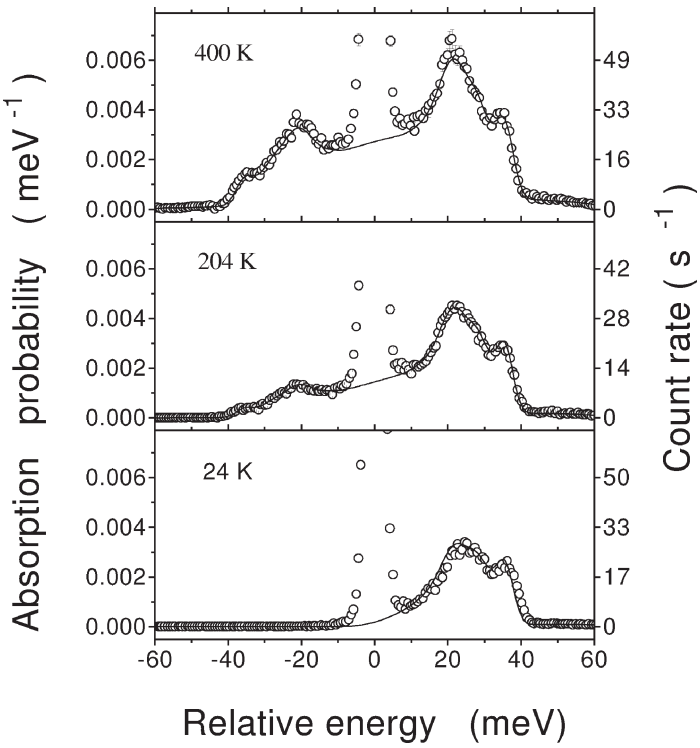

Figure 4. Energy spectra of nuclear inelastic absorption in α-iron at various temperatures. The solid lines are the calculations according to eqs. (7)–(9) with the density of phonon states at room temperature, obtained from neutron scattering [42] (from [23]).

3-yl) pyridine [47]. The electronic structure of the sample experiences a transition from a high-spin to a low-spin state when the temperature decreases below $\sim$173 K [47]. This transition is accompanied by a drastic change in the density of phonon states [1]. In the high-spin state the main peak of the phonon density of states is around 20–30 meV, whereas in the low-spin state it is shifted to $\sim$40–60 meV and contains a more pronounced fine structure. This development is clearly seen in the energy spectra of nuclear inelastic absorption (figure 5).

Even in the absence of a phase transition the temperature dependence of nuclear inelastic absorption cannot be completely attributed to the temperature variation of the occupation probability, because the density of phonon states still varies slightly with temperature due to the anharmonism of lattice vibrations. The inter-atomic potential is not symmetric, therefore the variation in the thermal energy changes the inter-atomic distances and forces. This introduces the corresponding change in the phonon density of states. Figure 6 shows the density of phonon states in α-iron at $T = 24$ K and $T = 400$ K [23]. The variation of the density of phonon states may be approximated by $\sim$4% “stretching” of the spectrum along the energy axis.

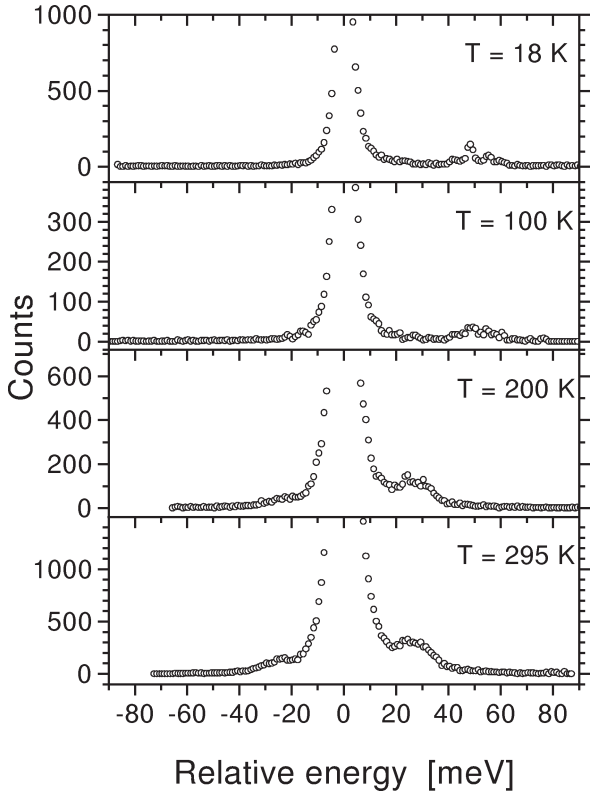

Figure 5. Energy spectra of nuclear inelastic absorption in the $[^{57}Fe(bpp)_2][BF_4]_2$ sample at various temperatures (from [30]).

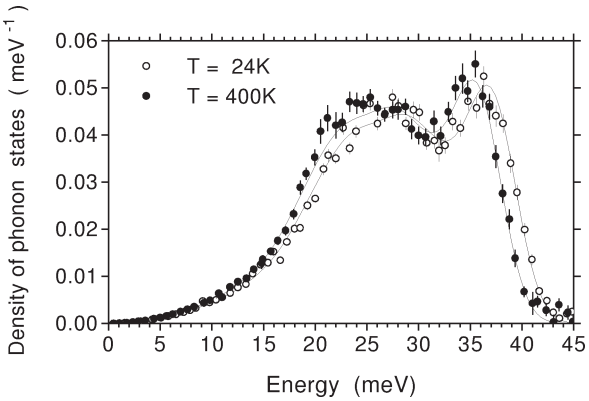

Figure 6. Density of phonon states in α-iron at 24 K and 400 K. The solid lines are obtained from the density of phonon states, derived from neutron studies at room temperature [42], which were convoluted with a Gaussian distribution of 4.4 meV width (FWHM) and fit to the data by "stretching" along the energy axis (from [23]).

7. Thermodynamic properties

The precise measurement of the densities of phonon states is one of the main merits of nuclear inelastic absorption. The knowledge of the density of phonon states allows one to calculate several thermodynamic parameters as specific heat, entropy, Lamb–Mössbauer factor, Debye temperature. Here we give two examples on the application of nuclear inelastic absorption for the determination of the Lamb–Mössbauer factor and the specific heat of α-iron. The measurements of the entropy for nanocrystalline iron were recently reported in [22].

As discussed above, the Lamb–Mössbauer factor may be calculated directly from the area of the energy spectrum, or from the derived density of phonon states. This gives a convenient tool to check the reliability of the data. Figure 7 shows the temperature dependence of the Lamb–Mössbauer factor in α-iron [23]. The data obtained from the two methods are in a good agreement with each other. The solid line shows the calculated Lamb–Mössbauer factor *for various temperatures* on the basis of the density of phonon states at *room temperature*, obtained from neutron scattering [42]. Neutron data coincide with the results of nuclear absorption not only at room temperature, but within the complete temperature range. This shows that the Lamb–Mössbauer factor has only a very weak sensitivity to the variation of the density of phonon states. However, this sensitivity may be followed, for instance, in the calculations of the Lamb–Mössbauer factor for zero temperature. Figure 8 shows the Lamb–Mössbauer factor of α-iron at *zero temperature*, calculated from the densities of phonon states, measured at *various temperatures*. Extrapolating the data to zero temperature, we estimated the Lamb–Mössbauer factor of α-iron at $T = 0$ as 0.9255(10).

The account of the temperature dependence of the density of phonon states is also important for the calculation of the specific heat. The lattice contribution to the

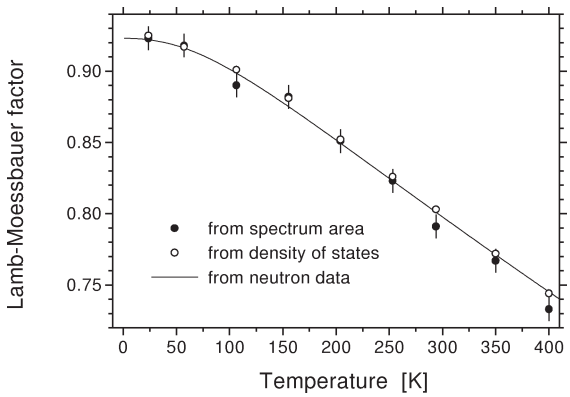

Figure 7. Temperature dependence of the Lamb–Mössbauer factor in α-iron, derived from nuclear inelastic absorption [23]. Filled circles represent the data calculated from the energy spectrum according to eq. (10); open circles those from the derived densities of phonon states according to eq. (2). The solid line is the calculation, based on the density of phonon states at room temperature, obtained from neutron scattering [42].

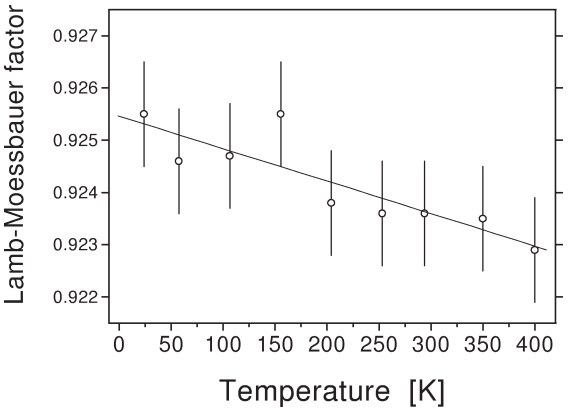

Figure 8. Lamb–Mössbauer factor of α-iron at zero temperature, calculated from the densities of phonon states at various temperatures [23]. The solid line is a linear fit.

specific heat at constant volume C_{V} for any given temperature may be calculated as [48]:

$$C_{\mathrm{V}}(T) = 3N_{\mathrm{A}}k_{\mathrm{B}}\int_0^\infty g(E,T)\frac{(\beta E)^2 \mathrm{e}^{\beta E}}{(\mathrm{e}^{\beta E}-1)^2}\,\mathrm{d}E, \tag{11}$$

where N_{A} is the Avogadro number. In order the compare the calculations with calorimetric data one needs the value of the specific heat at constant pressure C_{P}. The difference $C_{\mathrm{P}} - C_{\mathrm{V}}$ arises from the anharmonism of the lattice vibrations. Therefore the calculation of C_{P} requires not only the knowledge of the density of phonon states at the particular temperature, but also the temperature evolution of the density of phonon states. If the density of phonon states vary with temperature slowly, one may keep only the linear term in the temperature expansion of $C_{\mathrm{P}} - C_{\mathrm{V}}$. It has been shown [49], that in this approximation the specific heat at constant pressure is derived as:

$$C_{\mathrm{P}} = C_{\mathrm{V}}\left(1 - T\frac{1}{\nu}\frac{\mathrm{d}\nu}{\mathrm{d}T}\right), \tag{12}$$

where the term $(1/\nu)\cdot(\mathrm{d}\nu/\mathrm{d}T)$ is the mean relative change of the lattice vibration frequency with temperature. It can be calculated from the temperature dependence of the density of phonon states. Then the lattice contribution to the specific heat at constant pressure C_{P} may be derived and compared to the calorimetric data. The residual between the lattice contribution and the total specific heat may be attributed to the electronic specific heat.

Figure 9 shows the result of these calculations for the α-iron sample. In the temperature range 24–200 K the electronic specific heat C_{E} follows the expected linear law $C_{\mathrm{E}} = \gamma T$, where $\gamma = 5.0\times10^{-3}\ \mathrm{J\,mol^{-1}K^{-2}}$ is known from the low-temperature measurements [51]. However, at higher temperatures the electronic specific heat increases faster. A similar tendency was observed earlier for copper in neutron scattering [49], where it was suggested to originate from an additional quadratic term in the tem-

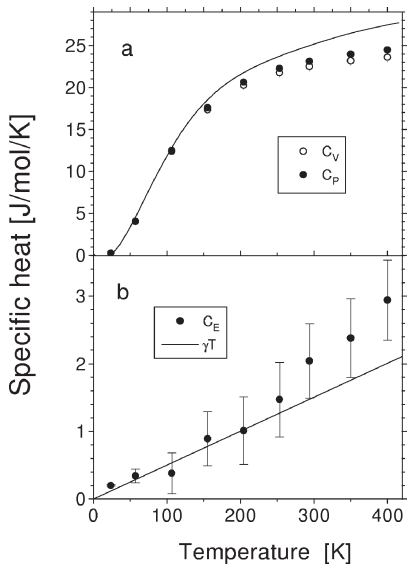

Figure 9. (a) Temperature dependence of the lattice specific heat (C_{V} and C_{P}) of α-iron, calculated from the densities of phonon states at various temperatures [23]. The solid line shows the calorimetric data on C_{P} from [50]. (b) Electronic specific heat C_{E} of α-iron. Solid line shows the expected γT dependence.

perature expansion of $C_{\mathrm{P}} - C_{\mathrm{V}}$. For α-iron the deviation of the electronic specific heat from γ T (figure 9) exceeds the $C_{\mathrm{P}} - C_{\mathrm{V}}$ contribution, therefore one hardly can attribute it to the next terms in eq. (12). We also can exclude as an explanation impurities (the purity of the material was $\sim$99.991% by weight [23]) and lattice vacancies [49] (the highest temperature was $\leqslant$25% of the melting point). One may search the reason of the observed deviation in the magnetic contribution to the specific heat capacity.

8. Sensitivity to the direction of lattice vibrations

Inelastic interaction of X-rays with nuclei is sensitive to the direction of lattice vibrations. This is obvious from the fact, that the energy of a photon in the reference system of a vibrating nucleus is determined by the projection of the velocity of the nucleus to the wave vector of the photon. The sensitivity of nuclear inelastic absorption to the polarization of lattice vibrations is hidden in studies of polycrystalline samples due to averaging over the various orientation of crystallites. However, it may be revealed with single crystals, where the energy spectra of lattice vibrations can be studied separately along different crystallographic directions.

We have performed these measurements with a ferric borate $^{57}FeBO_3$ single crystal, which has a calcite-type structure with $R\overline{3}c$ space group [52]. Energy spectra of nuclear inelastic absorption were measured for several polar angles θ and azimuthal angles φ between the incident X-ray beam and the [1 1 1] axis (figure 10). The energy

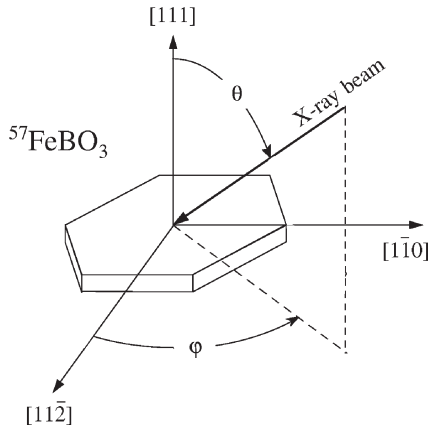

Figure 10. Orientation of the incident X-ray beam relative to the $FeBO_3$ crystal.

spectra revealed a pronounced dependence on the polar angle and no dependence on an azimuthal angle [25]. The Lamb–Mössbauer factors for various directions of the incident X-ray beam and the corresponding densities of phonon states were calculated.

The derived densities of phonon states in this case represent the frequency distributions of lattice vibrations along the specific crystallographic direction. Formally they are obtained from usual densities of states, which are weighted by the projection of the phonon polarization vector to the direction of the X-ray beam [27]. These "projected" densities of states for several crystallographic directions in the ferric borate crystal are shown in figure 11. The vibrations *perpendicular* to the [1 1 1] axis have one main characteristic energy of ∼22 meV (figure 11a). The energy spectrum of the vibrations *along* the [1 1 1] axis has an additional peak at 30 meV (figure 11e). These peaks indicate the most probable energies of the phonons, which likely result from the low-dispersive parts of the dispersion relations, where the phonon energy does not depend much on the phonon momentum.

In contrast to the pronounced anisotropy of the projected densities of states, the calculated Lamb–Mössbauer factors do not depend on the crystal orientation within the experimental uncertainty. For all directions they equal 0.81(2). Although this is a surprise, it is not a contradiction. The Lamb–Mössbauer factor is not very sensitive to the details of the density of phonon states. It is determined mostly by the low-energy part of the density of states; and one can see that all densities of states look similar below 25 meV (figure 11). From the methodological point of view, the observed combination of the pronounced anisotropy of the density of phonon state and the isotropic Lamb–Mössbauer factor provides a striking example of the advantages of the inelastic absorption technique compared to Mössbauer spectroscopy, where the Lamb–Mössbauer factor is the only parameter in order to study the lattice dynamics.

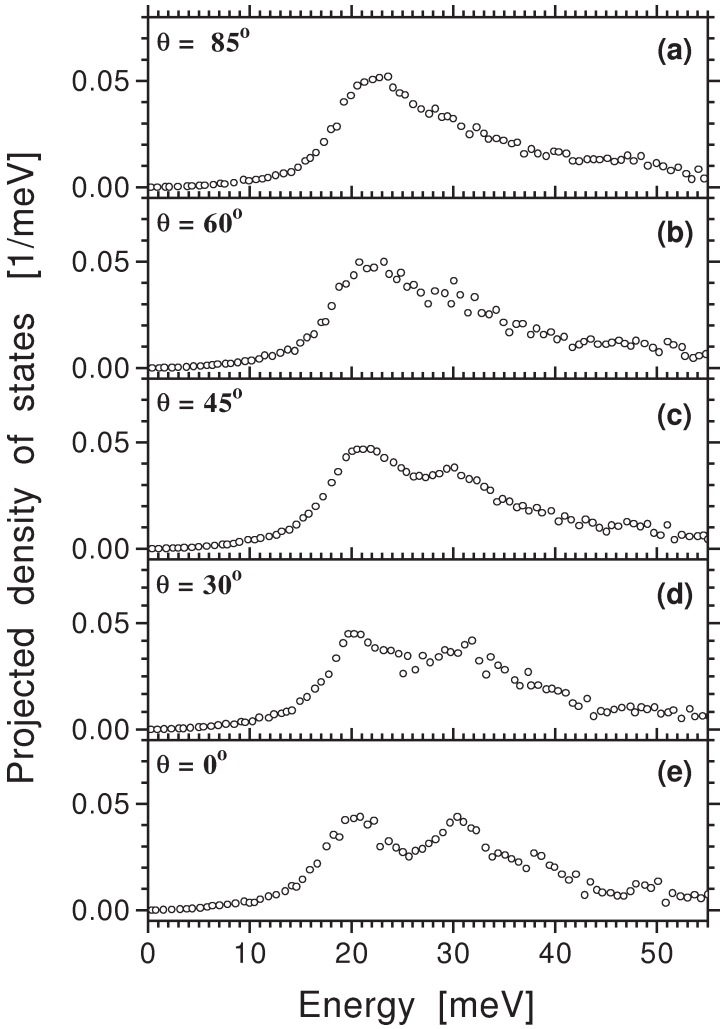

Figure 11. The projected densities of phonon states along several crystallographic directions of the $FeBO_3$ crystal. The polar angle θ is indicated in the figure. The azimuthal angle was $\varphi = 90^\circ$ (from [25]).

9. Site selectivity and averaging

By definition, nuclear inelastic absorption is only sensitive to the vibrations of the Mössbauer nuclei. It provides the energy spectrum of the vibrations of the selected atoms in the unit cell, i.e., the *partial* density of phonon states. Thus in contrast to inelastic neutron or X-ray scattering, nuclear inelastic absorption is the site-selective technique, because the "instrument" for the energy analysis (nuclear resonance) is a "built-in" feature of the sample.

However, synchrotron radiation experiment offers a helpful option to investigate both the dynamics of the selected atoms and the "averaged" dynamics of the lattice si-

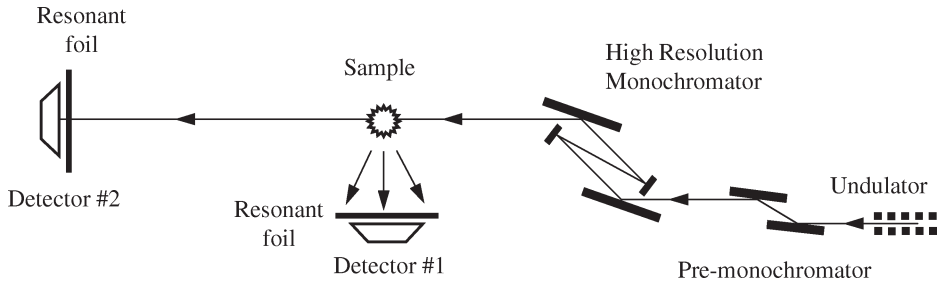

Figure 12. Experimental set-up for the measurements of inelastic X-ray scattering with nuclear resonant energy analysis of the scattered radiation.

multaneously. This comparison is especially valuable for the samples with complicated lattices (e.g., proteins), where the vibrations of the resonant atoms differ considerably from the "averaged" vibrations of the lattice [19,20,53]. For this purpose one needs to separate the "instrument" and the "sample", and to use the nuclear resonance in order to analyze the energy of the radiation, which is inelastically scattered by the non-Mössbauer atoms [54].

The experimental set-up for these measurements is shown in figure 12. The photons experience inelastic X-ray scattering in the sample and irradiate the foil of resonant isotope in front of the first detector. If in the process of inelastic X-ray scattering the energy of the incident photon is shifted to match the energy of nuclear resonance, this event produces the delayed signal in the detector. The second detector, as in the previous set-up (figure 1), measures the instrumental function of the monochromator.

The examples of nuclear resonance energy analysis of inelastic X-ray scattering is shown in figure 13. The energy distributions of X-rays scattered by water, Plexiglas, and gaseous xenon were measured [54]. The presence of inelastic scattering is clearly seen in a considerable broadening and in long tails of the energy spectra of scattered radiation relative to the instrumental function (dashed lines). The solid lines show the fit to the experimental data using a phenomenological approach (a), the density of states obtained in neutron studies (b), and a Doppler broadening model (c) (see [54] for the details).

10. Conclusion

During the first three years of its development Nuclear Inelastic Scattering passed the way from the first observation to an elaborated experimental technique. The main advantages of this method are the relatively simple experimental set-up, the precise measurement of the density of phonon states, and a high count rate, which allows one to use small (few mg) amounts of the material. The available sub-meV monochromators provide a perfect energy resolution to investigate the lattice dynamics of most substances. On the way to further improvement one may consider the technique of tunable μeV spectrometer [55]. Up to now most of the measurements were performed with the ^{57}Fe isotope, however, first inelastic measurements with ^{119}Sn [13,14,56] and

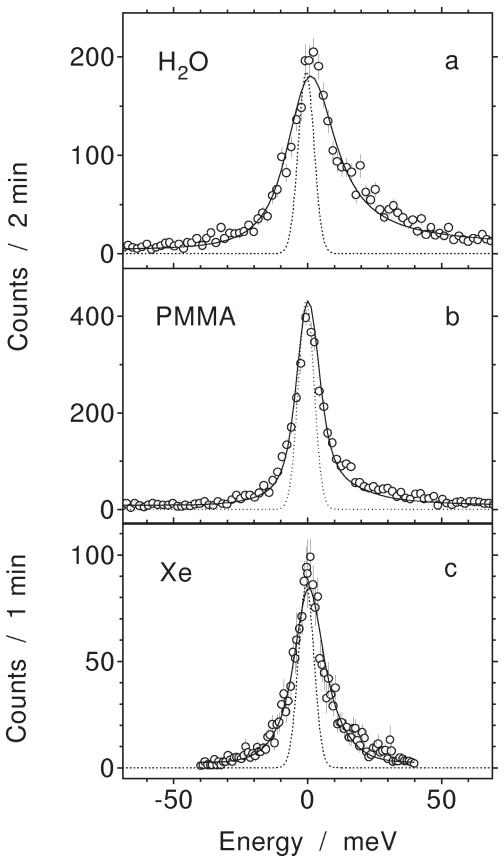

Figure 13. Energy spectra of inelastic X-ray scattering by water, PMMA, and gaseous Xe. The dashed lines show the instrumental function. The solid lines are the fit to the experimental data (from [54]).

^{151}Eu [57] have already started. In the nearest future one may expect further progress with ^{149}Sm and ^{161}Dy. In summary, nuclear inelastic scattering likely will become one of the most powerful techniques to study the dynamics of the matter.

References

[1] R. Rüffer and A.I. Chumakov, Hyperfine Interactions 97–98 (1996) 589.
[2] W.M. Visscher, Ann. Physics. 9 (1960) 194.
[3] E. Gerdau, R. Rüffer, H. Winkler, W. Tolksdorf, C.P. Klages and J.P. Hannon, Phys. Rev. Lett. 54 (1985) 835.
[4] G. Faigel, D.P. Siddons, J.B. Hastings, P.E. Haustein, J.R. Grover, J.P. Remeika and A.S. Cooper, Phys. Rev. Lett. 58 (1987) 2699.
[5] T. Ishikawa, Y. Yoda, K. Izumi, C.K. Suzuki, X.W. Zhang, M. Ando and S. Kikuta, Rev. Sci. Instr. 63 (1992) 1015.
[6] T.S. Toellner, T. Mooney, S. Shastri and E.E. Alp, in: *SPIE Proc.*, Vol. 1740, ed. J. Arthur (1992) p. 218.

[7] S. Kishimoto, Nucl. Instr. Meth. Phys. Res. A 309 (1991) 603.
[8] A.Q.R. Baron and S.L. Ruby, Nucl. Instr. Meth. Phys. Res. A 343 (1994) 517.
[9] U. Bergmann, J.B. Hastings and D.P. Siddons, Phys. Rev. B 49 (1994) 1513.
[10] J. Arthur, G.V. Smirnov, U. van Bürck, S.L. Ruby, A.Q.R. Baron, A.I. Chumakov and G.S. Brown, in: *Proc. of the Internat. Conf. on the Application of Mössbauer Effect*, Rimini (1995).
[11] G.V. Smirnov and V.G. Kohn, Phys. Rev. B 52 (1995) 3356.
[12] W. Sturhahn, K.W. Quast, T.S. Toellner, E.E. Alp, J. Metge and E. Gerdau, Phys. Rev. B 53 (1996) 171.
[13] M. Seto, Private communication.
[14] S. Kikuta, Hyperfine Interactions 90 (1994) 335.
[15] M. Seto, Y. Yoda, S. Kikuta, X.W. Zhang and M. Ando, Phys. Rev. Lett. 74 (1995) 3828.
[16] W. Sturhahn, T.S. Toellner, E.E. Alp, X.W. Zhang, M. Ando, Y. Yoda, S. Kikuta, M. Seto, C.W. Kimball and B. Dabrowski, Phys. Rev. Lett. 74 (1995) 3832.
[17] A.I. Chumakov, R. Rüffer, H. Grünsteudel, H.F. Grünsteudel, G. Grübel, J. Metge, O. Leupold and H.A. Goodwin, Europhys. Lett. 30 (1995) 427.
[18] X.W. Zhang, Y. Yoda, M. Seto, Yu. Maeda, M. Ando and S. Kikuta, Japan J. Appl. Phys. 34 (1995) L330.
[19] C. Keppler, K. Achterhold, A. Ostermann, U. van Bürck, W. Potzel, A.I. Chumakov, A.Q.R. Baron, R. Rüffer and F. Parak, European Biophys. J. 25 (1997) 221.
[20] T. Harami, G. Mijazaki, M. Seto, T. Mitsui, Y. Yoda, Y. Kobajashi, S. Kikuta and X.W. Zhang, to be published.
[21] S. Kikuta, Y. Yoda, I. Kojama, T. Shimizu, H. Igarashi, K. Izumi, Y. Kunimune, M. Seto T. Mitsui, T. Harami, X. Zhang and M. Ando, in: *X-ray and Inner-Shell Processes, Proc. of the 17th Internat. Conf.*, eds. R.L. Johnson, H. Schmidt-Böcking and B.F. Sonntag, AIP Conf. Proc. 389 (Woodbury, New York, 1996) p. 351.
[22] B. Fultz, C.C. Ahn, E.E. Alp, W. Sturhahn and T.S. Toellner, Phys. Rev. Lett. 79 (1997) 937.
[23] A.I. Chumakov, R. Rüffer, A.Q.R. Baron, H. Grünsteudel and H.F. Grünsteudel, Phys. Rev. B 54 (1996) 9596.
[24] M. Seto, Y. Yoda, S. Kikuta, X.W. Zhang and M. Ando, Il Nuovo Cimento D 18 (1996) 381.
[25] A.I. Chumakov, R. Rüffer, A.Q.R. Baron, H. Grünsteudel, H.F. Grünsteudel and V.G. Kohn, Phys. Rev. B 56 (1997) 10758.
[26] K.S. Singwi and A. Sjölander, Phys. Rev. 120 (1960) 1093.
[27] V.G. Kohn, A.I. Chumakov and R. Rüffer, unpublished.
[28] A.Q.R. Baron, Nucl. Instr. Meth. Phys. Res. A352 (1995) 665.
[29] A.Q.R. Baron, R. Rüffer and J. Metge, Nucl. Instr. Meth. Phys. Res. A400 (1997) 124.
[30] A.I. Chumakov, R. Rüffer, A.Q.R. Baron, J. Metge, H. Grünsteudel and H.F. Grünsteudel, in: *SPIE Proc.*, Vol. 3151, ed. A.T. Macrander (1997) p. 262.
[31] J.B. Hastings, D.P. Siddons, U. van Bürck, R. Hollatz and U. Bergmann, Phys. Rev. Lett. 66 (1991) 770.
[32] U. van Bürck, D.P. Siddons, J.B. Hastings, U. Bergmann and R. Hollatz, Phys. Rev. B 46 (1992) 6207.
[33] G.E. Bacon, *Neutron Diffraction* (Clarendon Press, Oxford, 1975).
[34] E. Burkel, *Inelastic Scattering of X-rays with Very High Energy Resolution* (Springer, New York, 1991).
[35] F. Sette, G. Ruocco, M. Krisch, U. Bergmann, C. Masciovecchio, V. Mazzacurati, G. Signorelli and R. Verbeni, Phys. Rev. Lett. 75 (1995) 850.
[36] A.I. Chumakov, J. Metge, A.Q.R. Baron, H. Grünsteudel, H.F. Grünsteudel, R. Rüffer and T. Ishikawa, Nucl. Instr. Meth. A 383 (1996) 642.
[37] T.S. Toellner, M.Y. Hu, W. Sturhahn, K. Quast and E.E. Alp, Appl. Phys. Lett. 71 (1997) 2112.

[38] J. Metge, K.W. Quast, O. Leopold, A.I. Chumakov, W. Sturhahn, R. Rüffer and E. Gerdau, in: *Proc. of the Internat. Conf. on the Application of Mössbauer Effect*, Rio de Janeiro (1997).
[39] A.I. Chumakov, J. Metge, A.Q.R. Baron, R. Rüffer, Yu.V. Shvydko, H. Grünsteudel and H.F. Grünsteudel, Phys. Rev. B 56 (1997) 8455.
[40] B. Sepiol, A. Meyer, G. Vogl, R. Rüffer, A.I. Chumakov and A.Q.R. Baron, Phys. Rev. Lett. 76 (1996) 3220.
[41] A. Sjölander, Arkiv för Fysik 14 (1958) 315.
[42] V.J. Minkiewicz, G. Shirane and R. Nathans, Phys. Rev. 162 (1967) 528.
[43] Y.A. Izyumov and N.A. Chernoplekov, *Neutron Spectroscopy* (Consultants Bureau, New York, 1994) p. 257.
[44] H.J. Lipkin, Ann. Physics 9 (1960) 332.
[45] T.S. Toellner, Ph.D. thesis, Northwestern University (1996).
[46] H.J. Lipkin, Phys. Rev. B 52 (1995) 10073.
[47] H.A. Goodwin and K.H. Sugiyarto, Chem. Phys. Lett. 139 (1987) 470.
[48] F.C.Brown, *The Physics of Solids* (Benjamin, New York, 1967) p. 182.
[49] A.P. Miller and B.N. Brockhouse, Canad. J. Phys. 49 (1971) 704.
[50] W. Auer, in: *Kalorische Zustandsgrössen*, eds. K. Schäfer and E. Lax, Landolt-Börnstein, Auflage 6, Band 2, Teil 4 (Springer, Berlin, 1961) pp. 478, 482.
[51] N.W. Ashcroft and N.D. Mermin, *Solid State Physics* (Saunders College, Philadelphia, 1976) p. 48.
[52] R. Diehl, Solid State Commun. 17 (1975) 743.
[53] K. Achterhold, C. Keppler, U. van Bürck, W. Potzel, P. Schindelmann, E.-W. Knapp, B. Melchers, A.I. Chumakov, A.Q.R. Baron, R. Rüffer and F. Parak, European Biophys. J. 25 (1996) 43.
[54] A.I. Chumakov, A.Q.R. Baron, R. Rüffer, H. Grünsteudel, H.F. Grünsteudel and A. Meyer, Phys. Rev. Lett. 76 (1996) 4258.
[55] R. Röhlsberger, E. Gerdau, R. Rüffer, W. Sturhahn, T.S. Toellner, A.I. Chumakov and E.E. Alp, Nucl. Instr. Meth. Phys. Res. A349 (1997) 251.
[56] A.I. Chumakov, A. Barla, R. Rüffer, J. Metge, H.F. Grünsteudel, H. Grünsteudel, J. Plessel, H. Winkelmann and M.M. Abd-Elmeguid, Phys. Rev. B 58 (1998) (in press).
[57] O. Leupold, Private communication.